

A Reliable Approach for Modeling the Actual Antenna Pattern in Millimeter-Wave Communication

Fulvio Babich and Massimiliano Comisso

Abstract—This letter presents a mathematical framework for evaluating the link capacity of an interfered communication link in a millimeter-wave mobile scenario, accounting in detail for the shape of the antenna pattern and for the statistic of the direction of arrivals. The developed approach, whose accuracy is verified by Monte Carlo validations in 2D and 3D wireless environments, does not require simplified antenna models, thus enabling to maintain the actual pattern during the analysis.

Index Terms—Millimeter-wave communication, antenna radiation pattern, interference, direction of arrival, link capacity.

I. INTRODUCTION

THE growing interest towards millimeter-wave (mmWave) technology has led to the development of several proposals [1]–[8], for analyzing and improving the functionalities enabled by the IEEE 802.15.3c and 802.11ad standards [9], [10]. Within these proposals, the antenna pattern plays a fundamental role, since the small size of the radiating elements operating in the 60 GHz band has made feasible the use of antenna arrays on the communication devices, thus enabling spatial reuse by beamforming operations [11]. However, to maintain the analytical tractability of a considered problem, the pattern shape is often simplified. The most common pattern approximations adopt circular sectors [1], infinitesimal beamwidths [2], flat-topped geometries [3]–[5], and directional models [6]–[8].

These approximations idealize many aspects of a real pattern, whose shape may be in general much more complex than that assumed in the commonly adopted simplified models. In fact, this shape may include transition zones and ripples in the main lobe, grating and secondary lobes, and narrow or large null regions [12]. The difference between ideal and actual pattern may introduce considerable discrepancies between theoretical and practical results. Therefore, a more realistic pattern may be introduced to improve the reliability of the analysis. This adoption however makes difficult to derive closed-form expressions for an investigated link quality metric, such as, for example, the success probability. Thus, a modeling strategy capable to guarantee the analytical tractability of a considered problem maintaining the actual shape of the pattern during the analysis may represent a desirable advance.

To deal with this issue, this letter proposes a theoretical approach for an accurate modeling of the antenna pattern in 2D and 3D scenarios. The approach is applied to a problem of link capacity estimation in an interfered multipath-fading environment. Monte Carlo validations are used to verify the accuracy

of the developed framework, which furthermore provides, in some specific cases, expressions available in analytical form.

The letter is organized as follows. Section II introduces the network scenario. Section III presents the pattern modeling approach and the capacity analysis. Section IV discusses the numerical results. Section V summarizes the main conclusions.

II. SCENARIO

Consider a wireless network in which a destination D is located at the center O of a ball $B_\nu(O, \bar{R})$ of radius \bar{R} and dimension $\nu \in \{2, 3\}$. This destination communicates with its desired source S lying at a distance $\hat{R} (\leq \bar{R})$ in the presence of L interferers uniformly distributed in $B_\nu(O, \bar{R})$, that is, on a disk for $\nu = 2$, and in a ball for $\nu = 3$. Accordingly, the cumulative density function (cdf) of the distance R_l between D and the l -th interferer may be expressed as [13]:

$$F_{R_l}(r_l) = \frac{1}{\bar{R}^\nu} \begin{cases} 0 & r_l < 0 \\ r_l^\nu & 0 \leq r_l \leq \bar{R} \\ \bar{R}^\nu & r_l > \bar{R} \end{cases} \quad (1)$$

In reception, D adopts a normalized antenna power gain pattern $\mathcal{P}(\omega)$, which is obtained from a broadside array and where the direction ω is the azimuth angle $\phi \in \Omega_2 = [0, 2\pi)$ for $\nu = 2$, and the zenith-azimuth pair $(\theta, \phi) \in \Omega_3 = [0, \pi] \times [0, 2\pi)$ for $\nu = 3$. In particular, a uniform linear array (ULA) of N elements lying on the x -axis is adopted for $\nu = 2$, while a uniform square array (USA) of $N \times N$ elements lying on the $x - z$ plane is adopted for $\nu = 3$. Thus, to jointly model the 2D and 3D cases, $\mathcal{P}(\omega)$ may be represented by [12]:

$$\mathcal{P}(\omega) = \prod_{j=1}^{\nu-1} \frac{\left| \sin \left[N\pi d S_j^{(\nu)}(\omega) \right] \right|^2}{\left| N \sin \left[\pi d S_j^{(\nu)}(\omega) \right] \right|^2}, \quad (2)$$

where d is the inter-element distance expressed as a multiple of the carrier wavelength λ , and:

$$S_j^{(\nu)}(\omega) = \begin{cases} \cos \phi & j = 1, \nu = 2 \\ \sin \theta \cos \phi & j = 1, \nu = 3 \\ \cos \theta & j = 2, \nu = 3 \end{cases} \quad (3)$$

The propagation channel is characterized by path-loss attenuation and multipath-fading. More precisely, the path-loss function is:

$$\varrho(r_l) = (r_l^\alpha + \epsilon)^{-1}, \quad (4)$$

where $\alpha (> 2)$ is the path-loss exponent and ϵ is a nonnegative parameter that identifies a classic unbounded path-loss model for $\epsilon = 0$ and a bounded path-loss model for $\epsilon > 0$. For each source (desired or interfering), a probability density function (pdf) $f_Q(q)$ models the power fluctuation Q due to fading, and

Manuscript received April 1, 2015; revised June 12, 2015; accepted June 12, 2015. The associate editor coordinating the review of this paper and approving it for publication was T. Yioultis.

The authors are with the Dipartimento di Ingegneria e Architettura (DIA), University of Trieste, 34100 Trieste, Italy (e-mail: mcomisso@units.it).

Digital Object Identifier 10.1109/LCOMM.2015.2445764

83 another pdf $f_{\Omega'}(\omega')$ models the spreading of the direction of
84 arrival (DOA) Ω' due to multipath. More precisely, $f_{\Omega'}(\omega')$
85 is selected as a Laplacian distribution, whose reliability in
86 describing the spatial channel has been assessed by several
87 measurement campaigns [14]. Hence, the pdf of the DOA may
88 be expressed for $\nu \in \{2, 3\}$ as [14]:

$$f_{\Omega'}(\omega') = \begin{cases} K_\nu \exp(-|\rho^{(\nu)}(\omega')|) & \omega' \in \Omega_\nu \\ 0 & \text{otherwise} \end{cases} \quad (5)$$

89 where K_ν is a normalization constant, and:

$$\rho^{(\nu)}(\omega') = \left(\frac{2}{\sigma^2}\right)^{\frac{\nu-1}{2}} \cdot \begin{cases} \phi - \pi & \nu = 2 \\ (\theta - \pi/2)(\phi - \pi) & \nu = 3 \end{cases} \quad (6)$$

90 with σ denoting the angular spread. For $\nu = 3$, (5) is modeled
91 as the product of two univariate Laplacian pdfs, thus assuming,
92 as in [14], the separability of the zenith and azimuth statistics.

93

III. ANALYSIS

94 The analysis of the described scenario requires two steps.
95 The first one provides a probability mass function (pmf) of
96 an equivalent gain that jointly models $\mathcal{P}(\omega)$ and $f_{\Omega'}(\omega')$. The
97 second step provides a parametric family of link capacity
98 values, each obtained for a given gain, which are subsequently
99 weighed according to the pmf, so as to evaluate the overall link
100 capacity by applying the concept of mixture distribution [15].

101 A. Pattern-DOA Statistic Modeling

102 As a first step, one has to derive the equivalent pattern [16]:

$$g(\omega) = \int_{\Omega_\nu} \mathcal{P}(\omega') f_{\Omega'}(\omega' - \omega) d\omega', \quad (7)$$

103 which enables to jointly account for the receiving pattern and
104 the DOA statistic within a unique function by averaging each
105 value of $\mathcal{P}(\omega)$ over the pdf $f_{\Omega'}(\omega')$. Since ω is the realization
106 of a random variable (r.v.) Ω , also the equivalent gain may
107 be viewed as a r.v. G . In general, $\mathcal{P}(\omega)$, and hence $g(\omega)$, are
108 not invertible functions of ω , thus the statistic of G cannot
109 be derived in closed-form, and an approximated strategy must
110 be developed. To this aim, one may recall that $\mathcal{P}(\omega)$ is a
111 normalized pattern and that $f_{\Omega'}(\omega')$ is a pdf, thus the values
112 of $g(\omega)$ belong to the interval $[0, 1]$. This interval may be
113 subdivided into $M - 1$ adjacent subintervals of equal length
114 $\chi = 1/(M - 1)$, to obtain the set of points $\mathbf{G} = \{g_i : g_i = (i -$
115 $1)\chi, i = 1, \dots, M\}$. The number of directions towards which
116 the equivalent gain is equal to g_i may be evaluated as $\#(\Xi_i)$,
117 which denotes the cardinality of the set $\Xi_i = \{\omega : g(\omega) = g_i\}$.
118 Therefore, observing that Ξ_1, \dots, Ξ_M is a sequence of disjoint
119 sets, the pmf of G may be estimated as:

$$f_G(g_i) = \frac{\#(\Xi_i)}{\sum_{i=1}^M \#(\Xi_i)}, \quad g_i \in \mathbf{G}. \quad (8)$$

120 The proposed pattern modeling approach has the considerable
121 advantage of modeling $\mathcal{P}(\omega)$ and $f_{\Omega'}(\omega')$ by a unique r.v., whose
122 accuracy in describing $g(\omega)$ may be controlled through the
123 number of gain samples M , which may be increased to allow
124 a more reliable modeling of the actual statistic of $g(\omega)$.

B. Link Capacity

125

Once the pmf of $g(\omega)$ is available, the interference analysis
126 may be carried out for a given value g_i , that is, assuming the
127 equivalent gain as constant. To this purpose, using (4), the
128 power received by the destination D from the l -th interferer for
129 a gain g_i in absence of mobility may be expressed as: 130

$$T_l = k g_i \varrho(R_l) = k g_i (R_l^\alpha + \epsilon)^{-1}, \quad (9)$$

where k is a constant accounting for the height of the antennas
131 and for the transmission power (assumed equal for all sources).
132 The cdf of T_l for a given g_i may be evaluated by inverting (9)
133 with respect to R_l and using (1), thus obtaining: 134

$$F_{T_l}(t_l; g_i) = \begin{cases} 0 & t_l < g_i \varsigma_1 \\ 1 - \frac{1}{R^v} \left(\frac{k g_i}{t_l} - \epsilon \right)^\beta & g_i \varsigma_1 \leq t_l \leq g_i \varsigma_2 \\ 1 & t_l > g_i \varsigma_2 \end{cases} \quad (10)$$

where $\beta = v/\alpha$, $\varsigma_1 = k \varrho(\bar{R})$, and $\varsigma_2 = k \varrho(0)$. Recalling that
135 $f_Q(q)$ is the pdf of Q that models the fading effects, the cdf of
136 $P_l = T_l Q$ may be derived from the product distribution [13]: 137

$$F_{P_l}(p_l; g_i) = \int_0^{+\infty} f_Q(q) F_{T_l}\left(\frac{p_l}{q}; g_i\right) dq, \quad (11)$$

which can be exploited to obtain the statistic of the total inter-
138 ference I . Usually, the pdf of I cannot be evaluated in closed-
139 form, and hence approximations based on the nearest interferers
140 have been introduced [2], [3]. In particular, according to [2], I
141 may be usefully approximated by: 142

$$I = \sum_{l=1}^L P_l \approx H_L^{(1/\beta)} \max\{P_1, \dots, P_L\}, \quad (12)$$

where $H_L^{(1/\beta)} = \sum_{l=1}^L l^{-1/\beta}$ is the generalized harmonic num-
143 ber of order L in power $1/\beta$. Using the relationship for the
144 scaling of r.v.s [13], the cdf and the pdf of I for a given g_i may
145 be hence calculated, respectively, from: 146

$$F_I(p; g_i, L) \cong \left[F_{P_l}\left(\frac{p}{H_L^{(1/\beta)}}; g_i\right) \right]^L, \quad (13)$$

$$f_I(p; g_i, L) = \frac{dF_I}{dp}. \quad (14)$$

Recalling that \hat{R} denotes the S-D distance and that the maxi-
147 mum of $g(\omega)$ is steered towards S, the desired signal power may
148 be expressed as $\Delta = \hat{t} Q$, where $\hat{t} = k \max\{g(\omega)\} \varrho(\hat{R})$. Hence,
149 the corresponding pdf is $f_\Delta(\delta) = f_Q(\delta/\hat{t})/\hat{t}$. This latter statistic
150 enables to obtain the cdf of the signal-to-interference ratio (SIR)
151 $\Upsilon = \Delta/I$ from the ratio distribution [13]: 152

$$F_\Upsilon(v; g_i, L) = 1 - \frac{1}{\hat{t}} \int_0^{+\infty} f_Q\left(\frac{\delta}{\hat{t}}\right) F_I\left(\frac{\delta}{v}; g_i, L\right) d\delta. \quad (15)$$

The result of the S-D communication may be then established
153 adopting a SIR threshold ψ that accounts for modulation,
154 coding, packet length, and required packet error rate [4], [8].
155 Thus, the capture probability for a given g_i is evaluated as: 156

$$\eta(\psi; g_i, L) = \Pr\{v > \psi\} = 1 - F_\Upsilon(\psi; g_i, L). \quad (16)$$

157 It is interesting to observe that, in the presence of Rayleigh
 158 fading, the pdf of I and the capture probability for $L = 1$ may
 159 be represented in analytical form. To this aim, evaluating (11)
 160 for $f_Q(q) = e^{-q}u(q)$, where $u(\cdot)$ is the Heaviside step function
 161 with $u(0) = 0$, the cdf of P_I may be derived as:

$$F_{P_I}(p_I; g_i) = \int_{\frac{p_I}{g_i \zeta_2}}^{\frac{p_I}{g_i \zeta_1}} e^{-q} \left[1 - \frac{1}{\bar{R}^\nu} \left(\frac{k g_i q}{p_I} - \epsilon \right)^\beta \right] dq + \int_0^{\frac{p_I}{g_i \zeta_2}} e^{-q} dq, \quad (17)$$

162 which, recalling that $\zeta_1 = k/(\bar{R}^\alpha + \epsilon)$ and $\zeta_2 = k/\epsilon$, provides
 163 (18), shown at the bottom of the page, where $\gamma(\cdot, \cdot)$ is the lower
 164 incomplete gamma function [17]. Now, using (18) in (13)–(16),
 165 one may then obtain $f_I(p; g_i, L)$ in (19) and $\eta(\psi; g_i, 1)$ in (20),
 166 also, shown at the bottom of the page, where $\zeta_{L,\beta} = kH_L^{(1/\beta)}$
 167 and ${}_2F_1(\cdot, \cdot; \cdot; \cdot)$ is the hypergeometric function [17].

168 The capacity of the S-D link may be finally evaluated. To
 169 this purpose, the parametric family $\eta(\psi; g_i, L)$, resulting for $i =$
 170 $1, \dots, M$, is employed to derive the capture probability from
 171 the mixture distribution [15]:

$$\eta(\psi; L) = \sum_{i=1}^M \eta(\psi; g_i, L) f_G(g_i). \quad (21)$$

172 This latter expression may be used to estimate the limiting
 173 performance of the interfered link according to the Shannon
 174 bound, thus obtaining the link capacity as:

$$C(\psi; L) = \eta(\psi; L) \log_2(1 + \psi). \quad (22)$$

175 It is useful to notice that the proposed pattern modeling ap-
 176 proach allows one to account for the impact of $\mathcal{P}(\omega)$ and $f_{\mathcal{Q}'}(\omega')$
 177 not only on the link capacity, but on any quantity for which a
 178 parametric family of pdfs or cdfs has been calculated during
 179 the analysis. For example, one may evaluate, again from the
 180 mixture distribution, the pdf of the interference power as:

$$f_I(p; L) = \sum_{i=1}^M f_I(p; g_i, L) f_G(g_i). \quad (23)$$

181 Observe that the expressions in (21)–(23) together with those in
 182 (18)–(20) represent a significant result, since, even if the latter
 183 ones may seem formally elaborated, they have two relevant
 184 advantages that are uncommonly present at the same time in
 185 theoretical mmWave modeling: the maintenance of the actual
 186 pattern as it is, and the availability of analytical forms.

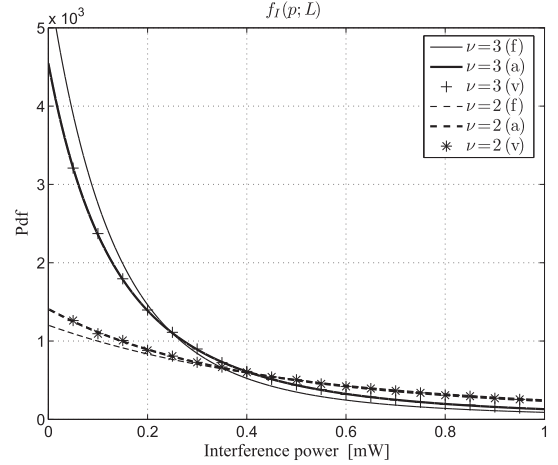


Fig. 1. Pdf of the interference in 2D and 3D cases for $\bar{R} = 2\hat{R} = 10$ m, $\epsilon = 1$, $L = 1$ (f: flat-topped pattern, a: actual pattern, v: Monte Carlo validation).

IV. RESULTS

187

The results are evaluated for $N = 4$, $d = 1/4$, $\alpha = 3$, $\sigma = 188$
 $\pi/3$, $\chi = 0.01$, $k = 1$ in a Rayleigh fading scenario, and are
 189 verified by Monte Carlo validations. Each analytical curve
 190 obtained from the actual pattern is compared with that obtained
 191 from a flat-topped pattern [3]–[5], in order to check the sensi-
 192 tivity of the results on the actual pattern details. According to
 193 the typical rules adopted to derive the flat-topped model of a
 194 given pattern, the flat-topped pattern is generated so as to have
 195 the main lobe width equal to the half-power beamwidth Ω_{3dB}
 196 of the actual pattern, the main lobe gain equal to the mean gain
 197 of the actual pattern inside Ω_{3dB} , and the back-lobe gain equal
 198 to the mean gain of the actual pattern outside Ω_{3dB} .
 199

Figs. 1 and 2 report the pdf of the interference power and the
 200 link capacity, respectively, for $\bar{R} = 2\hat{R} = 10$ m, $\epsilon = 1$, $L = 1$.
 201 The figures refer to the 2D case for a ULA of $N = 4$ elements,
 202 and to the 3D case for a USA of $N \times N = 4 \times 4$ elements. The
 203 significant matching between the analysis obtained from the
 204 actual pattern and the validation confirms the accuracy of
 205 the developed framework. Furthermore, this matching reveals
 206 that the characteristics of the actual pattern not included in its
 207 flat-topped model may have, mainly in the 3D case, a not negli-
 208 gible influence on the final results. This aspect is confirmed by
 209 Fig. 3, which is obtained for $\nu = 3$, $\bar{R} = 2\hat{R} = 10$ m, $\epsilon = 1$, and
 210 different L values, and by Fig. 4, which is obtained for $\nu = 3$,
 211 $\bar{R} = 2\hat{R} = 1$ m, $L = 1$, and different ϵ values. With reference
 212 to this latter figure, which shows the critical impact of the
 213

$$F_{P_I}(p_I; g_i) = \left\{ 1 - \exp\left(-\frac{\epsilon p}{k g_i}\right) \left[\exp\left(-\frac{\bar{R}^\alpha p}{k g_i}\right) + \left(\frac{k g_i}{\bar{R}^\alpha p}\right)^\beta \gamma\left(1 + \beta, \frac{\bar{R}^\alpha p}{k g_i}\right) \right] \right\} u(p_I) \quad (18)$$

$$f_I(p; g_i, L) \cong F_{P_I}^{L-1}\left(\frac{k p}{\zeta_{L,\beta}}; g_i\right) \exp\left(-\frac{\epsilon p}{g_i \zeta_{L,\beta}}\right) \left[\exp\left(-\frac{\bar{R}^\alpha p}{g_i \zeta_{L,\beta}}\right) \frac{\epsilon L}{g_i \zeta_{L,\beta}} + \frac{L (g_i \beta \zeta_{L,\beta} + \epsilon p)}{(g_i \zeta_{L,\beta})^{1-\beta} p^{1+\beta} \bar{R}^\nu} \gamma\left(1 + \beta, \frac{\bar{R}^\alpha p}{g_i \zeta_{L,\beta}}\right) \right] u(p) \quad (19)$$

$$\eta(\psi; g_i, 1) = \begin{cases} 1 - \beta k g_i \psi \left[\frac{\pi (\epsilon \hat{t} + k g_i \psi)^{\beta-1}}{\hat{t}^\beta \bar{R}^\nu \sin(\beta \pi)} - \frac{1}{(1-\beta) \hat{t} \bar{R}^\alpha} {}_2F_1\left(1, 1 - \beta; 2 - \beta; -\frac{\epsilon \hat{t} + k g_i \psi}{\hat{t} \bar{R}^\alpha}\right) \right] & 0 < \beta < 3/2, \beta \neq 1 \\ 1 - \frac{k g_i \psi}{\hat{t} \bar{R}^\alpha} \log\left(1 + \frac{\hat{t} \bar{R}^\alpha}{\epsilon \hat{t} + k g_i \psi}\right) & \beta = 1 \end{cases} \quad (20)$$

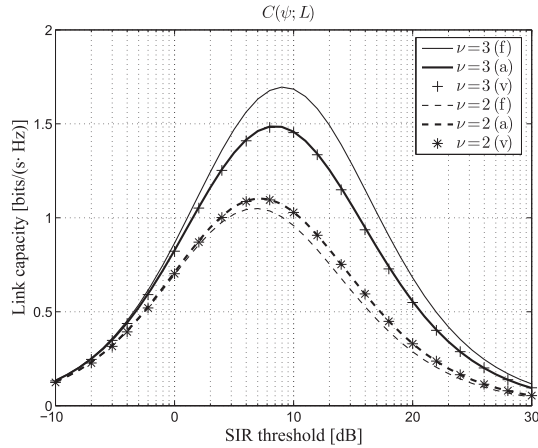


Fig. 2. Link capacity in 2D and 3D cases for $\bar{R} = 2\hat{R} = 10$ m, $\epsilon = 1$, $L = 1$ (f: flat-topped pattern, a: actual pattern, v: Monte Carlo validation).

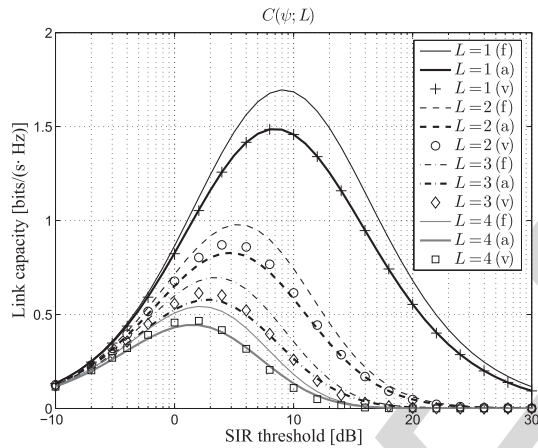


Fig. 3. Link capacity in 3D case for $\bar{R} = 2\hat{R} = 10$ m, $\epsilon = 1$, and different L values (f: flat-topped pattern, a: actual pattern, v: Monte Carlo validation).

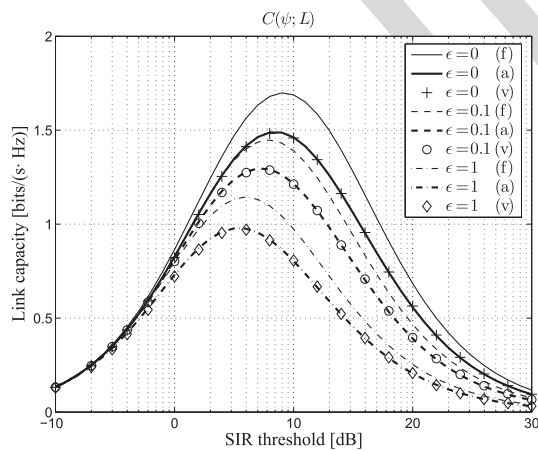


Fig. 4. Link capacity in 3D case for $\bar{R} = 2\hat{R} = 1$ m, $L = 1$, and different ϵ values (f: flat-topped pattern, a: actual pattern, v: Monte Carlo validation).

214 path-loss model in a short-range scenario, it is worth to no-
 215 tice that the far-field assumption is satisfied. In fact, consid-
 216 ering half-wavelength radiators and $d = 1/4$, the maximum
 217 dimension of the adopted USA of $N \times N$ elements is $D =$
 218 $\sqrt{2[N\lambda/2 + (N-1)\lambda/4]}$, with $\lambda = 5$ mm at 60 GHz. Thus,

since the far-field region begins at $2D^2/\lambda \cong 15$ cm [12], the 219
 far-field assumption may be considered satisfied. In summary, 220
 the presented results suggest that the proposed approach, com- 221
 bining the concepts of equivalent pattern and mixture distribu- 222
 tion, may represent a useful support for the analysis of some 223
 scenarios in which, even in the presence of other relevant 224
 phenomena, such as interference, path-loss attenuation, and 225
 multipath-fading, an investigated link quality metric turns out 226
 to be sensitive to the actual pattern details. 227

V. CONCLUSION

228

A mathematical approach for modeling the DOA statistic and 229
 the antenna pattern in 2D and 3D mmWave scenarios has been 230
 presented and exploited to derive the link capacity in an inter- 231
 ferred multipath-fading environment. Monte Carlo validations 232
 have confirmed the accuracy of the developed method, which 233
 enables to properly account for the actual pattern shape, and, 234
 in some specific cases, provides analytical expressions for the 235
 investigated performance figures. 236

REFERENCES

237

- [1] Q. Chen, J. Tang, D. T. C. Wong, X. Peng, and Y. Zhang, "Direc- 238
 tional cooperative MAC protocol design and performance analysis for 239
 IEEE 802.11ad WLANs," *IEEE Trans. Veh. Technol.*, vol. 62, no. 6, 240
 pp. 2667–2677, Jul. 2013. 241
- [2] F. Babich and M. Comisso, "Capture analysis of mobile multi-packet 242
 networks adopting spatial reuse: An alternative study," in *Proc. IEEE 243
 GLOBECOM*, 2014, pp. 3477–3482. 244
- [3] A. M. Hunter, J. G. Andrews, and S. Weber, "Transmission capacity of 245
 ad hoc networks with spatial diversity," *IEEE Trans. Wireless Commun.*, 246
 vol. 7, no. 12, pp. 5058–5071, Dec. 2008. 247
- [4] T. Bai and R. W. Heath, Jr., "Coverage and rate analysis for millimeter- 248
 wave cellular networks," *IEEE Trans. Wireless Commun.*, vol. 14, no. 2, 249
 pp. 1100–1114, Feb. 2015. 250
- [5] M. Kim, S.-E. Hong, and J. Kim, "Analysis of directional communication 251
 via relaying devices in mmWave WPANs," *IEEE Commun. Lett.*, vol. 16, 252
 no. 3, pp. 342–345, Mar. 2012. 253
- [6] Y. Wang, X. Kang, H. K. Garg, M. Motani, and Q. Chen, "Throughput 254
 maximization for 60 GHz WPANs via device cooperation," *IEEE 255
 Commun. Lett.*, vol. 18, no. 5, pp. 785–788, May 2014. 256
- [7] C.-S. Sum and H. Harada, "Scalable heuristic STDMA scheduling 257
 scheme for practical multi-Gbps millimeter-wave WPAN and WLAN 258
 systems," *IEEE Trans. Wireless Commun.*, vol. 11, no. 7, pp. 2658–2669, 259
 Jul. 2012. 260
- [8] S. Singh, R. Mudumbai, and U. Madhow, "Interference analysis for highly 261
 directional 60-GHz mesh networks: The case for rethinking medium 262
 access control," *IEEE/ACM Trans. Netw.*, vol. 19, no. 5, pp. 1513–1527, 263
 Oct. 2011. 264
- [9] *IEEE Std for High Rate WPANs MAC/PHY Specific. Amend. 2: Millimeter 265
 Wave Based Alternative PHY Ext.*, IEEE 802.15.3c, Oct. 2009. 266
- [10] *IEEE Std for WLAN MAC/PHY Specific. Amend. 3: Enhanc. for Very High 267
 Throughput in the 60 GHz Band*, IEEE 802.11ad, 2014. 268
- [11] J. G. Andrews et al., "What will 5G be?" *IEEE J. Sel. Areas Commun.*, 269
 vol. 32, no. 6, pp. 1065–1082, Jun. 2014. 270
- [12] C. A. Balanis, *Antenna Theory: Analysis and Design*. New York, NY, 271
 USA: Wiley, 1997. 272
- [13] R. D. Yates and D. J. Goodman, *Probability and Stochastic Processes*. 273
 New York, NY, USA: Wiley, 1999. 274
- [14] M. B. Knudsen and G. F. Pedersen, "Spherical outdoor to indoor power 275
 spectrum model at the mobile terminal," *IEEE J. Sel. Areas Commun.*, 276
 vol. 20, no. 6, pp. 1156–1169, Aug. 2002. 277
- [15] S. Frühwirth-Schnatter, *Finite Mixture and Markov Switching Models*. 278
 New York, NY, USA: Springer-Verlag, 2006. 279
- [16] F. Babich and M. Comisso, "Throughput and delay analysis of 802.11- 280
 based wireless networks using smart and directional antennas," *IEEE 281
 Trans. Commun.*, vol. 57, no. 5, pp. 1413–1423, May 2009. 282
- [17] M. Abramowitz and I. A. Stegun, *Handbook of Mathematical Func- 283
 tions with Formulas, Graphs, and Mathematical Tables*, ser. National 284
 Bureau of Standards: Applied Mathematics, Series 55. Gaithersburg, 285
 MD, USA: National Bureau of Standards, 1964. 286

AUTHOR QUERY

NO QUERY.

IEEE
Proof